Journal of the American Ceramic Society

Atomistic Modeling of Effect of Mg on Oxygen Vacancy Diffusion in α-Alumina

Journal:	*Journal of the American Ceramic Society*
Manuscript ID:	JACERS-34607.R1
Manuscript Type:	Article
Date Submitted by the Author:	17-Apr-2014
Complete List of Authors:	Tewari, Abhishek; Ecole Polytechnique Federal de Lausanne, Materials Science and Engineering Aschauer, Ulrich; ETH Zurich, Department of Materials Bowen, Paul; Ecole Polytechnique Federal de Lausanne, Materials Science and Engineering
Keywords:	alumina, atomistic simulation, sinter/sintering, diffusion/diffusivity, impurities

Atomistic Modeling of Effect of Mg on Oxygen Vacancy Diffusion in α-Alumina

Abhishek Tewari[a,1], Ulrich Aschauer[b], Paul Bowen[a]

[a]Powder Technology Laboratory, Institute of Materials Science, EPFL, CH-1015 Lausanne, Switzerland

[b]Materials Theory, Department of Materials, ETH Zurich, CH-8093 Zürich, Switzerland

Abstract

Oxygen diffusion plays an important role in grain growth and densification during the sintering of alumina ceramics and governs high temperature processes such as creep. The atomistic mechanism for oxygen diffusion in alumina is however still debated; atomistic calculations not being able to match experimentally determined activation energies for oxygen vacancy diffusion. These calculations are however usually performed for perfectly pure crystals, whereas virtually every experimental alumina sample contains a significant fraction of impurity/dopants ions. In the present study we use atomistic defect cluster and nudged elastic band calculations to model the effect of Mg impurities/dopants on defect binding energies and migration barriers. We find that oxygen vacancies can form energetically favorable clusters with Mg, which reduces the number of mobile species and leads to an additional 1.5 eV energy barrier for the detachment of a single vacancy from Mg. The migration barriers of diffusive jumps change such that an enhanced concentration of oxygen vacancies is expected around Mg ions. Mg impurities were also found to cause destabilization of certain vacancy configurations as well as enhanced vacancy-vacancy interaction.

[1] Corresponding author email: abhit1985@gmail.com

1. Introduction

Alumina (α-Al_2O_3) is one of the most important structural ceramics. Its excellent mechanical properties, biocompatibility and high temperature chemical inertness make it suitable for various applications, such as refractory, dental implants and abrasives. Knowledge of diffusion in alumina is crucial to understand high temperature processes such as diffusional creep, sintering of ceramics, plastic deformation of single crystals and alumina scale formation in Al containing alloys. Experimentally the oxygen self-diffusion coefficient in alumina is determined via O^{18} tracer diffusion or dislocation loop annealing experiments at different temperatures. The activation energy for oxygen diffusion in alumina was found to be 5-6 eV in several experimental studies using both these techniques[1]. Atomistic computational studies based on empirical potentials or first-principles however report the migration energy for oxygen vacancies in pure alumina to be 1-2 eV[2,3]. This failure to reconcile experimental and theoretical results for oxygen diffusion in alumina is popularly known as the conundrum of oxygen diffusion in corundum, a phrase coined in[4].

The formation energy for intrinsic oxygen Frenkel or Schottky defects in alumina is predicted to be about 5 eV[5,6], which is too high for a significant intrinsic defect concentration. The defect population in alumina is therefore believed to result from charge compensation around aliovalent impurities or dopants. Although diffusion experiments claim to use pure alumina, all samples contain varying levels of impurities (table 2 in[7]). Even the purest of alumina contains ppm levels of background impurities, like Ca^{2+}, Mg^{2+}, Si^{4+} or Ti^{4+}. Lagerlof and Grimes[5] have shown through static lattice calculations of defect energies coupled with mass action calculations that even such small amounts of impurities may control the defect chemistry in alumina. They further pointed out that excess as small as 2 ppm of bivalent or tetravalent impurities can result in a

change of the dominant type of defect (oxygen vacancy for Mg^{2+}, Al interstitials for Ti^{4+}) and important variations in the overall defect concentration. Hence no alumina sample can realistically be considered as undoped. In this perspective it may not seem surprising that independent experimental studies on undoped alumina with varying amount of impurities result in fairly consistent results. Moreover even results for bulk diffusion of oxygen in alumina vary only modestly between doped and undoped alumina[1,8,9,10] suggesting a strong contribution from extrinsic impurities. Heuer[1] termed this insensitivity as the buffering of oxygen diffusion in alumina.

Experimental and theoretical studies have attempted to understand the effect of dopants/impurities on the lattice[8,9,10] and grain boundary diffusion[11,12,13] of oxygen in alumina. Ti doping[9,10] is reported to decrease the bulk diffusion of oxygen while Mg either increases it[9] or leaves it unaffected[8]. In contradiction to what is expected from classical point defect chemistry[5], the magnitude of change in the diffusion coefficient is very small (50-100 times)[9]. It has been suggested that even in pure alumina impurities affect the concentration of 'available' mobile defects due to defect cluster formation[5,6,14]. Extra binding energy is needed to break the defect clusters and free the mobile defects for diffusion. The possibility of tightly bound cluster migration instead of free defect migration has also been postulated in the literature[9].

Earlier studies on the effects of dopants on the oxygen vacancy diffusion in other ionic solids (e.g. ceria and zirconia) have shown that the dopant concentration and distribution affect the diffusion process. Doping with aliovalent elements (Y in ZrO_2 and Sm, Gd in CeO_2) increases the ionic diffusivity at low temperatures and low dopant concentrations, with diffusivity reaching a maximum at an optimum dopant concentration in zirconia and ceria[15]. Vacancy-vacancy interaction as well as dopant-vacancy interaction resulting from effective net charge on the

defects and the elastic strain field could hinder the diffusion process through several mechanisms. At high concentrations, the formation of dopant pairs at nearest neighbor positions is assumed to increase the fraction of blocked sites for diffusion[16,17,18]. Formation of divacancy complexes in yttria stabilized zirconia could also render certain dopant-vacancy configurations unstable, in turn reducing the number of available diffusive pathways[16,19,20]. Ordering of defects is also expected due to dopant-vacancy interaction, making nearest neighbor configurations more stable for dopant-vacancy pairs[16,17].

In spite of previous studies on the effect of dopants/impurities on bulk oxygen diffusion in alumina it is still unclear how and to what extent impurities can account for the inconsistency between theoretical and experimental activation energies. In the present work we first calculate the migration barriers in pure alumina using nudged elastic band[21] and Metadynamics[22] methods based on empirical potentials to compare the accuracy of different methods (section 3.1). Thereafter, defect cluster formation energies and oxygen vacancy migration barriers in the neighborhood of an Mg impurity are calculated to characterize the effect of an Mg impurity on oxygen vacancy diffusion in alumina (sections 3.2 and 3.3). Other effects such as vacancy destabilization and vacancy-vacancy interaction are observed due to the presence of Mg, which are discussed in detail in sections 3.4 and 3.5.

2. Computational Method

The description of the energetics is based on the Born model for solids including long-range electrostatic interactions and short-range attractive and repulsive forces described by empirical Buckingham pair-potentials. A core-shell model[23] was adopted to account for the polarizable nature of the oxygen ions. The potential parameters developed by Lewis and Catlow[24] were used

in the present work and the bulk structure of α-alumina was taken from Liu et al.[25]. The General Utility Lattice Program (GULP)[26,27] was used for all defect and migration energy calculations. Defect energies were calculated using the Mott-Littleton approach with 10 Å and 25 Å for the radii of region 1 and 2 respectively, which leads to well-converged energies even for the largest clusters. Distance dependent binding energies between oxygen vacancies (denoted as V_O from here on) and an Mg impurity (denoted as Mg_{Al} from here on) were calculated by substituting Mg onto an Al site and subsequently creating one V_O at a time on all O sites within a 6 Å radius of the Mg. After structural relaxation, the binding energy was computed by subtracting the defect energies of the V_O and Mg_{Al} computed separately. Defect cluster energies were calculated similarly by creating an Mg_{Al} and multiple V_O's within a 6 Å radius of the Mg_{Al}. The average distance of the vacancy cluster was calculated as the mean of the distances of different V_O's from the Mg_{Al} and average defect binding energy per V_O was calculated to evaluate the effect of defect cluster composition on the binding energy.

Nudged elastic band (NEB)[21] calculations were performed in a periodic 3×3×1 supercell of the hexagonal alumina unit cell. This size represents a good tradeoff between avoiding spurious interaction with periodic images and an affordable computational cost. Two methods were tested to neutralize the 1e charge introduced by the combination of an Mg_{Al} and a V_O: Smearing of the excess charge over the Al sublattice or adding a neutralizing background charge. We found both options to give identical results for relative energies, such as binding energies and migration barriers. Migration barriers for a total of 208 diffusive jumps within a radius of 6 Å of the Mg_{Al} were calculated. Initial and final states for the NEB calculations were constructed by removing oxygen ions from the initial and final position of the V_O migration pathway respectively. After relaxation of these endpoint structures, NEB calculations were carried out using 10 intermediate

images to discretize the minimum energy pathway (MEP). The migration barrier of a jump is extracted as the difference in energy between the initial point and the highest energy point (transition state) of the pathway.

It should be noted here that the lower computational cost of the force field method in comparison to first principle DFT calculations allows us to consider fairly large (6 Å) defect cluster radii as well as a large number (208) of migration barrier calculations. To verify the accuracy of the force field, migration barriers in pure alumina were also calculated using DFT as well as with different potential sets[28] details being given in the supplementary material. This comparison shows that while absolute values for the diffusion dominating jumps can vary by ~0.5 eV for different computational methods (Figure S1), the relative changes induced by the presence of Mg are unaffected (Figure S2). Our results hence accurately capture the relative effects resulting from the presence of Mg, which is the focus of the present study.

3. Results and Discussion

3.1. Migration barriers in pure alumina

Oxygen vacancy diffusion in alumina has been computed by different methods in the past[3,7,14,29,30]. Due to the high migration barriers, metadynamics[22] and NEB calculations based either on first principles or empirical potentials were the most efficient. We performed a preliminary study to check the consistency of these two methods. As shown in previous work, three different classes of primary jumps for oxygen vacancies exist in bulk alumina[3,7]. The migration barriers for these three primary jumps were calculated using metadynamics and NEB based on empirical potentials. Details about the metadynamics calculations can be found in our earlier work[7]. We note here that due to an inappropriate choice of the collective variable

(anchoring to a fixed point instead of the center of mass of the remaining ions), migration barriers were largely overestimated in that work and we report corrected values in the following section. In figure 1 we show the migration barriers of the three classes of primary jumps computed using metadynamics and NEB. The metadynamics energy barriers slightly overestimate the NEB barriers, by an amount, which seems proportional to the barrier height. This is most likely due to the lack of directional resolution of the collective variable as discussed in[7].

Figure 1 (top panel) shows the schematic diagram of the three different classes of jumps. The first class of jumps with a jump distance of 2.42 Å has the lowest migration barrier but does not contribute to macroscopic diffusion because the V_O motion is restricted to a closed loop as previously discussed[3,7]. The second (2.52 Å) and third (2.67 Å) class of jumps form an interconnected network of jumps and could contribute to macroscopic diffusion. The second class of jumps will however not significantly contribute to diffusion due to its high migration energy; therefore diffusion predominantly occurs by the third class of jumps. The calculated migration barriers are in good agreement with previous calculations[2,3], but still much lower than the experimentally measured activation energies. As it yields more detailed information on the minimum energy pathway, we have chosen to use the NEB method in the remainder of this study.

3.2. Binding Energy of Oxygen Vacancies

The binding energy of V_O with Mg_{Al} decreases asymptotically with increasing distance as shown in figure 2. The highest binding energies of about 1.5 eV are observed for V_O located in nearest neighbor sites to Mg_{Al}. These binding energies are in good agreement with 1.36 eV reported by Lagerlof et al.[5] and to a lesser extent with 0.9 eV reported by Harding et al.[14]. The interaction

between the two defects is of very long range, still leading to an energy gain of 0.5 eV at 5 Å separation. It is important to note that not only the distance between Mg_{Al} and the V_O, but also the local configuration of the cluster determines the binding energy, as can be seen from the scatter in the data.

This implies that V_O will be strongly attracted by Mg_{Al} over a long distance. This attraction could dramatically decrease the number of mobile defects as an additional activation energy of ~1.5 eV is required for the detachment of V_O in nearest neighbor positions of Mg_{Al}.

This is in agreement with the predictions by Lagerlof et al.[5] that the positively charged cluster consisting of one Mg_{Al} and one V_O is dominant in samples with excess Mg^{2+} compared to Ti^{4+} impurities. Lagerlof et al.[9] also suggested that defect clusters formed in experimental pure alumina due to the presence of trace cation impurities could dominate the diffusion process and that an additional binding energy would need to be overcome to free the mobile defects for diffusion through V_O mechanism.

Given that a cluster of one Mg_{Al} and one V_O has a net positive charge it is interesting to verify if additional vacancies can still bind to this cluster. In figure 3, we therefore report the binding energy per V_O for clusters with an increasing number of V_O. The red data points are the same as in the previous figure and are repeated here for clarity. We can see that independent of the cluster size, arrangements restricted to the nearest neighbor shell (around 1.9 Å distance) of Mg_{Al} are energetically the most favorable. There are however only six of these nearest neighbor sites, which restricts the maximum number of favorably bound V_O while still retaining a reasonable coordination of the Mg_{Al}. This is reflected in the rapid increase in the magnitude of the binding energy with increasing number of V_O and the fact that beyond three V_O the nearest neighbor cluster becomes energetically unstable. For clusters with larger numbers of V_O the

accommodation in mixed nearest and next-nearest neighbor or clusters of even larger radius becomes more and more favorable. We note here that the formation of such highly charged clusters might seem counterintuitive at first. However one can construct a model by assuming coulomb energetics between relative charges of -1 (Mg_{Al}) and 2 (V_O), which are located on the surface of a sphere with radius equal to the Mg-O distance (1.8 Å). Using this model it can be shown that for two V_O the sum of attractive (Mg_{Al}-V_O) energies is still larger than the sum of repulsive (V_O-V_O) energies when the V_O are located at maximum possible separation (i.e. at opposite poles of the sphere). For three V_O the overall interaction within this model is slightly repulsive, indicating that either the atomistic geometry relaxes, resulting in the favorable interaction in figure 3 or that other energy contributions such as short-range forces also play a role. Our evaluation of clusters with a larger number of V_O and larger radii is restricted by the computational cost. It is therefore not impossible that an energetically favorable cluster with four V_O exists, however not with sites only in the nearest and next nearest neighbor shells.

We want to note here that besides the formation of V_O-Mg_{Al}-V_O clusters, Mg_{Al}-V_O-Mg_{Al} clusters may also form[5]. In the next section we will treat the effect of the former type or cluster on diffusion kinetics. To complement this discussion we show in the supporting information (S3) some preliminary results on the effect of the latter type of clusters on the diffusion kinetics. A complete evaluation is out of the scope of this work but will be an interesting topic for future research.

3.3. Effect of Mg on migration barriers

The effect of Mg_{Al} on the migration barrier of V_O jumps is characterized by three parameters: the initial distance between V_O and Mg_{Al}, whether the V_O moves ‘closer to’ or ‘away from’ Mg_{Al} and the migration trajectory.

Figure 4 a), b) and c) show the migration barriers for the jumps of class I, II and III, respectively in the presence of Mg_{Al}. Compared to undoped alumina the migration barriers for all three classes of jumps increase or remain unchanged if the vacancies move away from Mg_{Al}. For all three classes of jumps the migration barrier increases by up to a factor 2 for jumps where V_O moves from the first nearest neighbor position of Mg_{Al} to a farther position. On the other hand, the migration barrier is lower than in undoped alumina if the V_O approaches Mg_{Al}. The activation energy decreases by almost 4 times if V_O moves from a second nearest neighbor to a nearest neighbor position of Mg_{Al}, which is observed for jumps of class I and III.

In figure 5, we plot the data for jumps of the diffusion dominating class III as a function of the change in distance between V_O and Mg_{Al} in the saddle point state and the initial state. Negative values on the x-axis correspond to the jumps where V_O approaches Mg_{Al} in the saddle point state in comparison to initial state and positive values to jumps increasing the distance between the two. Some points on the negative side of x-axis have higher migration barriers than in undoped alumina. It should be noted however that the change in distance (0.1-0.2 Å) is fairly small for these points and except for two jumps, the change in the migration barrier is also very small (<0.1 eV). Therefore not only the initial and final distance of V_O from Mg_{Al}, but also the migration path affects the migration barrier of a particular jump.

The Brønsted-Evans-Polanyi relation was shown to relate thermodynamic and kinetic parameters of physical properties, such as diffusion and has the potential to be used as a predictive tool[31]. The validity of this relation was checked in the present context by plotting the migration barrier as a function of the energy difference between the initial and the final state for all class III jumps (figure 6). Although the linear fit to the data points is not perfect, it could likely serve as a predictive tool for diffusion activation barriers in alumina containing several cationic trace

impurities. The advantage of this approach would be the much-reduced computational cost of structural relaxations of the end-points compared to full nudged-elastic-band calculations.

These results show that Mg_{Al} also has a rather strong effect on the migration of the defects in its proximity, increasing migration barriers for jumps leading away by up to ~0.4 eV, whereas jumps approaching Mg_{Al} are favored by lowering of the migration barriers by up to ~0.5 eV for the diffusion dominating class III jumps. These alterations of the migration barriers kinetically favor an increased concentration of V_O in the vicinity of Mg_{Al} as was expected from the preceding energetic arguments and the condition of detailed balance.

3.4. Vacancy destabilization

Mg_{Al} was observed to render certain V_O positions unstable, the V_O moving to an adjacent site while relaxing the endpoint structure (figure 7 inset). This occurs only for V_O in second nearest neighbor positions to Mg_{Al} and the exchanges are restricted to sites linked by class I jumps. Structural relaxation due to the proximity of Mg_{Al} can hence implicitly carry out a class I jump.

These relaxations can lead to alterations of the diffusive pathways in close proximity of the Mg_{Al}. For some of the jumps, the minimum energy pathways exhibited two barriers separated by a metastable state (figure 7). Upon closer inspection this metastable state is revealed to be the original initial state, the V_O having relaxed to a lower energy state by spontaneously performing a class I jump under the influence of Mg_{Al}. For the V_O to go from the new initial state to the final state, it will pass by the metastable (the original initial) state. In doing so V_O will first reverse the class I jump, which has a higher energy than in pure alumina as the V_O is attracted by the Mg_{Al}. This is followed by the actual diffusive jump, the barrier of which can be larger or smaller than in pure alumina depending if the jump approaches or leads away from Mg_{Al} (see figure 4). A schematic view of the relaxation and the two-step diffusive jump is shown in the inset in figure

7. Pietrucci et al.[19] reported a similar destabilization of V_O due to the presence of yttrium in yttrium-stabilized zirconia (YSZ).

It is interesting to note that vacancy destabilization not only divides a single step diffusive jump into two concerted jumps but also enhances the overall migration barrier of the full migration. E.g. a jump of class III, which previously had a barrier of ~0.9 eV will have a combined barrier of up to ~2.2 eV due to this vacancy destabilization and relaxation process as shown by the blue solid curve in figure 7.

3.5. Vacancy-vacancy interaction effects

The aforementioned likelihood of V_O cluster formation around Mg_{Al} makes it necessary to consider the effect of V_O-V_O interaction on migration barriers. In order to gain some preliminary insights on this interaction, a particular V_O jump was carried out in presence of one additional V_O at different nearest neighbor sites. The migration barrier for this particular jump in presence of Mg but without a second vacancy was ~1eV. In figure 8 we can see different effects of the second V_O on the minimum energy pathway: 1) the presence of a second V_O at two different positions (black lines) destabilizes the initial V_O position, leading to metastable states, and 2) depending on the position, the second V_O can either increase (red lines), leave unaffected (grey line) or decrease (blue line) the energy barrier. These observations are similar to what Pietrucci et al.[20] observed for V_O-V_O interaction in YSZ. They reported these interactions to destabilize a large number of V_O cluster configurations and to strongly affect migration barriers depending on the relative position of the other vacancies. These V_O-V_O interaction effects are governed by long-range electrostatic and medium-range elastic interactions due to the relaxation patterns around vacancies. As shown by Pietrucci[20], the correct treatment of these elastic interactions in YSZ requires fairly large simulation cells. In our Mott-Littleton calculations we found however

that at a distance of 10 Å from the V_O, atomic displacements were smaller than 0.005 Å, showing that elastic effects in alumina might be of shorter range than in YSZ. This gives us the confidence that results obtained in our chosen supercell should be reliable.

4. Summary and Conclusions

The migration barriers for oxygen vacancies, thought to be the dominating diffusion vehicle in pure alumina, were found to be in the range of 0.8 – 1.5 eV, which is much lower than the experimental values (5-6 eV). The migration barriers calculated using two different methods, Nudged Elastic Band and the Metadynamics, were found to be consistent. This and the agreement with previous work suggest that our model captures the vacancy behavior in a pure alumina system. We then went on to look at the effect of an Mg impurity or dopant to see if this can account for the difference between experiment (non-pure alumina) and previous theory (pure alumina).

Substitutional magnesium (Mg_{Al}) defects lead to an energetically favorable binding of up to three oxygen vacancies (V_O). The first V_O can bind with an energy of ~1.5 eV whereas the binding energy is reduced by more than half for each subsequent V_O. V_O are most favorably accommodated in nearest neighbor positions to Mg_{Al} but the electrostatic interaction is of very long range and leads to energetically favorable clusters with larger radii (up to 6Å radius were considered here). This implies that Mg_{Al} impurities and dopants will capture an important number of V_O in their vicinity, thus reducing the number of available mobile defects and modifying the transport mechanism. High binding energies of the defect clusters also point towards the possibility of a tightly bound cluster migration mechanism for diffusion in alumina.

Mg_{Al} also affects the migration barriers of V_O in alumina. Migration barriers of the jumps towards Mg_{Al} decrease by a factor 4, whereas those away have their barriers increased by a

factor of 2. This will also kinetically favor an enhanced concentration of V_O in the vicinity of Mg_{Al}.

Given that the effect of an increased barrier and the binding energy are additive to the migration energy of V_O, Mg_{Al} may account for a 2-3 eV increase in the total migration barrier of a diffusive jump of oxygen vacancies in the vicinity of Mg impurity. Certain vacancy positions were rendered unstable due to the presence of Mg as well as due to the vacancy-vacancy interaction, which converts single diffusive jumps into two subsequent jumps with an overall increase in the migration barrier also. This will further modify diffusion energetics, as was reported for yttrium stabilized zirconia[19].

This leads to the picture that Mg dopants and impurities in alumina lead to a reduction of the number of mobile V_O's due to an enhanced V_O concentration in the vicinity of Mg impurities. On the other hand Grimes and Lagerlöf[5] showed that Mg excess dramatically increases the number of V_O's. The diffusion coefficient is hence determined by a competitive effect between the increased total number of defects and their modified mobility in the region of the dopants or impurities.

In conclusion dopants or impurities have a significant influence on the V_O diffusion process in alumina. Our results indicate that the impurity population found in experimental alumina systems will contribute significantly to the high experimental values for diffusion activation energies, when compared to those calculated in atomistic simulations of pure alumina. Future modeling work, needs to focus on three key issues: 1) taking into account other cation impurities present in experimental alumina, 2) investigating the possibility of tightly bound cluster migration in alumina, and 3) developing simulation methods to quantify the effect of impurities on 'macroscopic' diffusion in alumina.

Acknowledgements

The authors would like to thank the Swiss National Science Foundation SNF Project No. 200020_144499 for the financial support for the current work.

References

[1] A.H. Heuer, "Oxygen and aluminum diffusion in [alpha]-Al_2O_3: How much do we really understand?," *J. Eur. Ceram. Soc.*, **28** [7] 1495–1507 (2008).

[2] C. Catlow, R. James, W. Mackrodt, and R. Stewart, "Defect energetics in α-Al_2O_3 and rutile TiO_2," *Phys. Rev. B*, **25** [2] 1006–1026 (1982).

[3] P.W.M. Jacobs and E.A. Kotomin, "Defect energies for pure corundum and for corundum doped with transition metal ions," *Philos. Mag. A*, **68** [4] 695 (1993).

[4] A.H. Heuer and K.P.D. Lagerlöf, "Oxygen self-diffusion in corundum (alpha-Al_2O_3): a conundrum," *Philos. Mag. Lett.*, **79** [8] 619 (1999).

[5] K.P.D. Lagerlöf and R.W. Grimes, "The defect chemistry of sapphire ([alpha]-Al_2O_3)," *Acta Mater.*, **46** [16] 5689–5700 (1998).

[6] K. Matsunaga, T. Tanaka, T. Yamamoto, and Y. Ikuhara, "First-principles calculations of intrinsic defects in Al_2O_3," *Phys. Rev. B*, **68** [8] 085110 (2003).

[7] U. Aschauer, P. Bowen, and S.C. Parker, "Oxygen vacancy diffusion in alumina: New atomistic simulation methods applied to an old problem," *Acta Mater.*, **57** [16] 4765–4772 (2009).

[8] K.P.R. Reddy and A.R. Cooper, "Oxygen Diffusion in Sapphire," *J. Am. Ceram. Soc.*, **65** [12] 634–638 (1982).

[9] K.P.D. Lagerlof, T.E. Mitchell, and A.H. Heuer, "Lattice Diffusion Kinetics in Undoped and Impurity-Doped Sapphire (alpha-Al_2O_3): A Dislocation Loop Annealing Study," *J. Am. Ceram. Soc.*, **72** [11] 2159–2171 (1989).

[10] H. Haneda and C. Monty, "Oxygen Self-Diffusion in Magnesium- or Titanium-Doped Alumina Single Crystals," *J. Am. Ceram. Soc.*, **72** [7] 1153–1157 (1989).

[11] H. Yoshida, S. Hashimoto, and T. Yamamoto, "Dopant effect on grain boundary diffusivity in polycrystalline alumina," *Acta Mater.*, **53** [2] 433–440 (2005).

[12] T. Nakagawa, I. Sakaguchi, N. Shibata, K. Matsunaga, T. Mizoguchi, T. Yamamoto, H. Haneda, and Y. Ikuhara, "Yttrium doping effect on oxygen grain boundary diffusion in [alpha]-Al_2O_3," *Acta Mater.*, **55** [19] 6627–6633 (2007).

[13] T. Matsudaira, M. Wada, T. Saitoh, and S. Kitaoka, "Oxygen permeability in cation-doped polycrystalline alumina under oxygen potential gradients at high temperatures," *Acta Mater.*, **59** [14] 5440–5450 (2011).

[14] J.H. Harding, K.J.W. Atkinson, and R.W. Grimes, "Experiment and Theory of Diffusion in Alumina," *J. Am. Ceram. Soc.*, **86** [4] 554–59 (2003).

[15] P.-L. Chen and I.-W. Chen, "Grain Growth in CeO2: Dopant Effects, Defect Mechanism, and Solute Drag," *J. Am. Ceram. Soc.*, **79** [7] 1793–1800 (1996).

[16] D. Marrocchelli, P.A. Madden, S.T. Norberg, and S. Hull, "Structural Disorder in Doped Zirconias, Part II: Vacancy Ordering Effects and the Conductivity Maximum," *Chem. Mater.*, **23** [6] 1365–1373 (2011).

[17] A. Ismail, J. Hooper, J.B. Giorgi, and T.K. Woo, "A DFT+U study of defect association and oxygen migration in samarium-doped ceria," *Phys. Chem. Chem. Phys.*, **13** [13] 6116 (2011).

[18] P.P. Dholabhai, S. Anwar, J.B. Adams, P. Crozier, and R. Sharma, "Kinetic lattice Monte Carlo model for oxygen vacancy diffusion in praseodymium doped ceria: Applications to materials design," *J. Solid State Chem.*, **184** [4] 811–817 (2011).

[19] F. Pietrucci, M. Bernasconi, C. Di Valentin, F. Mauri, and C.J. Pickard, "EPR g-tensor of paramagnetic centers in yttria-stabilized zirconia from first-principles calculations," *Phys. Rev. B*, **73** [13] 134112 (2006).

[20] F. Pietrucci, M. Bernasconi, A. Laio, and M. Parrinello, "Vacancy-vacancy interaction and oxygen diffusion in stabilized cubic ZrO_2 from first principles," *Phys. Rev. B*, **78** [9] 094301 (2008).

[21] H. Jónsson, G. Mills, and K. Jacobsen, "Nudged elastic band method for finding minimum energy paths of transition"; pp. 385–404 in *Class. Quantum Dyn. Condens. Phase Simul.* World Scientific, 1998.

[22] A. Laio and M. Parrinello, "Escaping free-energy minima," *Proc. Natl. Acad. Sci.*, **99** [20] 12562–12566 (2002).

[23] B.G. Dick and A.W. Overhauser, "Theory of the Dielectric Constants of Alkali Halide Crystals," *Phys. Rev.*, **112** [1] 90–103 (1958).

[24] G.V. Lewis and C.R.A. Catlow, "Potential models for ionic oxides," *J. Phys. C Solid State Phys.*, **18** [6] 1149–1161 (1985).

[25] R.S. Liu, W.C. Shi, Y.C. Cheng, and C.Y. Huang, "Crystal structures and peculiar magnetic properties of α- And γ-Al_2O_3 powders," *Mod. Phys. Lett. B*, **11** [26-27] 1169–1174 (1997).

[26] J.D. Gale and A.L. Rohl, "The General Utility Lattice Program (GULP)," *Mol. Simul.*, **29** [5] 291–341 (2003).

[27] E.R. Cope and M.T. Dove, "Pair distribution functions calculated from interatomic potential models using the *General Utility Lattice Program*," *J. Appl. Crystallogr.*, **40** [3] 589–594 (2007).

[28] D.J. Binks, "Computational Modelling of Zinc Oxide and Related Oxide Ceramics."; University of Surrey, Guildford, UK, 1994.

[29] J. Carrasco, N. Lopez, and F. Illas, "First Principles Analysis of the Stability and Diffusion of Oxygen Vacancies in Metal Oxides," *Phys. Rev. Lett.*, **93** [22] 225502 (2004).

[30] Y. Lei, Y. Gong, Z. Duan, and G. Wang, "Density functional calculation of activation energies for lattice and grain boundary diffusion in alumina," *Phys. Rev. B*, **87** [21] 214105 (2013).

[31] L. Bellarosa, N. Lopez, and K. Honkala, "Adsorbate-Induced Oxygen Vacancy Mobility in Ultrathin Oxide Films," *J. Phys. Chem. C*, **117** [45] 23806–23811 (2013).

List of Figures

Figure 1. (Top) Schematic diagram of the three classes of diffusive jumps of oxygen vacancies in alumina (reprinted from ref.[7] with permission). (Bottom) Migration barriers for the three classes of primary jumps, computed using the nudged elastic band (NEB, solid lines) and metadynamics (MTD, dashed lines) methods. For NEB the whole minimum energy pathway is given, while for MTD only the height of the saddle point is indicated.

Figure 2. Binding energy of the V_O and Mg_{Al} as a function of their distance. The blue line is a 1/d fit to the data.

Figure 3. Binding energy per V_O for defect clusters of one Mg_{Al} and one to four V_O. Negative values indicate energetically favorable binding.

Figure 4. Migration barriers for the diffusive jumps of oxygen vacancies as a function of the initial distance of the oxygen vacancy from Mg for primary jumps of (a) class I (2.42 Å), (b) class II (2.54 Å) and (c) class III (2.65 Å). Dashed lines are the migration barriers in pure alumina for the respective class of jumps.

Figure 5. Migration barriers of class III diffusive jumps as a function of the difference in the initial and saddle point distance of the V_O from Mg_{Al}. Negative values on the x-axis represent jumps where V_O approaches Mg_{Al}. The dashed line is the migration barrier in pure alumina.

Figure 6. Brønsted-Evans-Polanyi plot. Migration barriers for the class III diffusive jumps plotted as a function of the energy difference between the initial and the final state of the vacancy. The straight line is a linear fit to the data points.

Figure 7. Minimum energy pathways for jumps starting from vacancy positions, which became unstable due to the presence of Mg_{Al}. The inset shows a schematic view of the relaxation process leading from the metastable (m) position to the new initial (i) position. Going from the new initial (i) position to the final (f) position now requires two diffusive jumps going via the intermediate metastable (m) state. This two-step nature is reflected by the two barriers observed in the minimum energy pathways (MEPs). The lines are cubic splines interpolated between NEB images. Red and blue solid curves are the MEPs of the highest barrier class II and class III jumps, respectively from this initial position. Red and blue dotted lines are the remaining class II and class III jumps respectively.

Figure 8. Minimum energy pathways showing the effect of V_O-V_O interaction by addition of a second V_O at different nearest neighbor sites. The dashed horizontal line is the migration barrier of the jump without a second V_O. Pathways with a destabilized initial position are shown in black, those with an increase in barrier in red, the one with an unaffected barrier in grey and the one with a lower barrier in blue. The lines are cubic splines interpolated between NEB images.

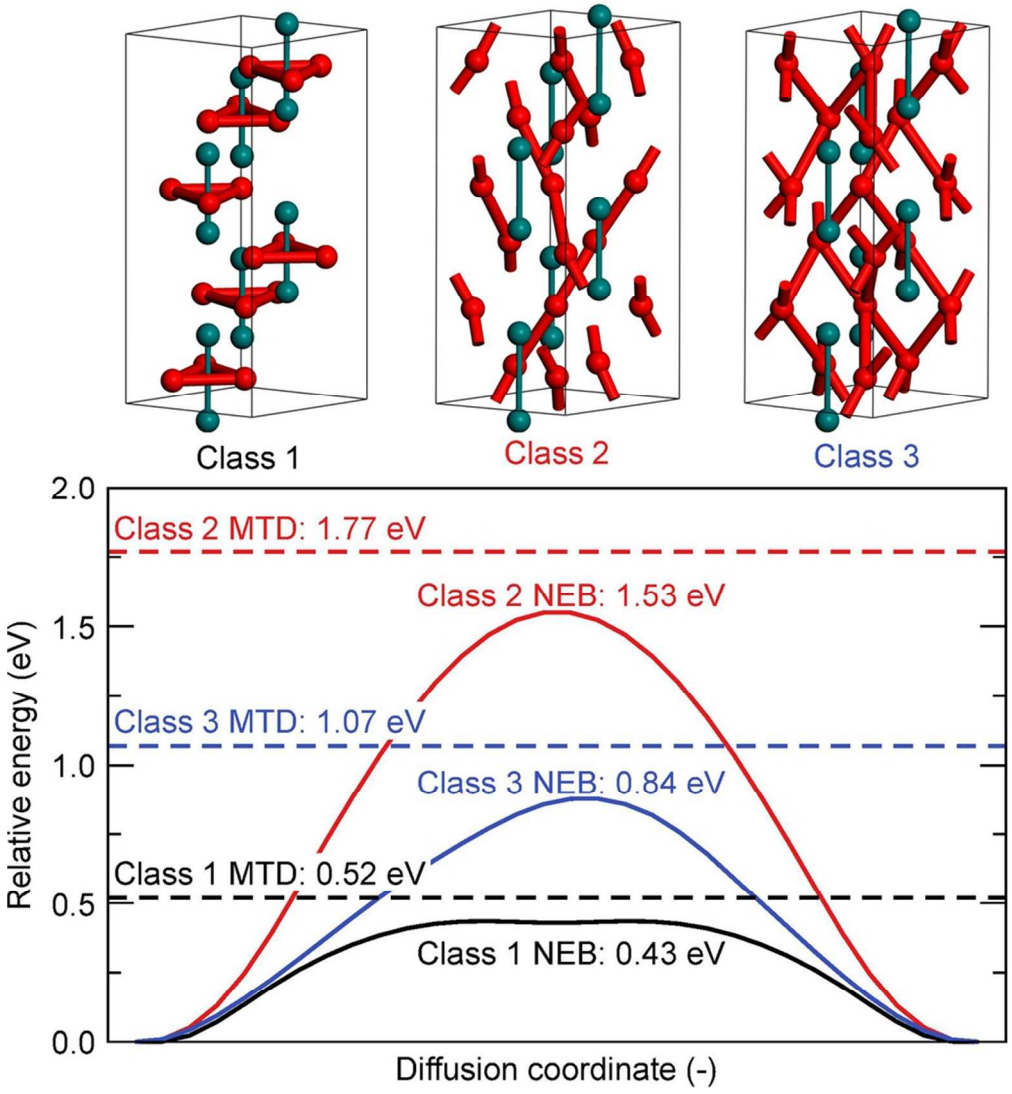

Figure 1. (Top) Schematic diagram of the three classes of diffusive jumps of oxygen vacancies in alumina (reprinted from ref.7 with permission). (Bottom) Migration barriers for the three classes of primary jumps, computed using the nudged elastic band (NEB, solid lines) and metadynamics (MTD, dashed lines) methods. For NEB the whole minimum energy pathway is given, while for MTD only the height of the saddle point is indicated.
86x94mm (300 x 300 DPI)

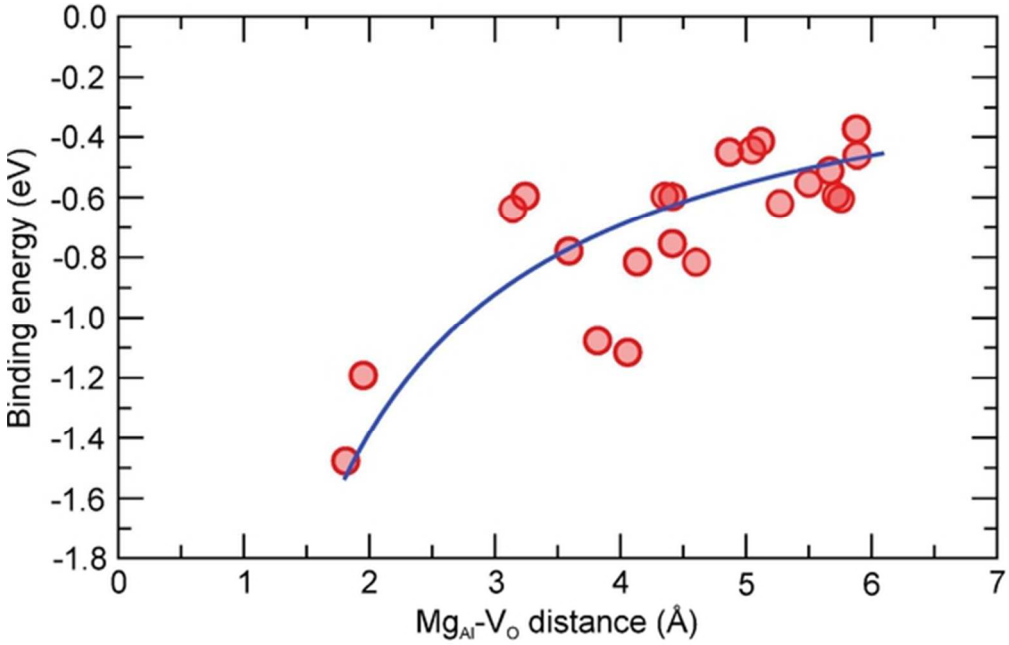

Figure 2. Binding energy of the VO and MgAl as a function of their distance. The blue line is a 1/d fit to the data.
51x32mm (300 x 300 DPI)

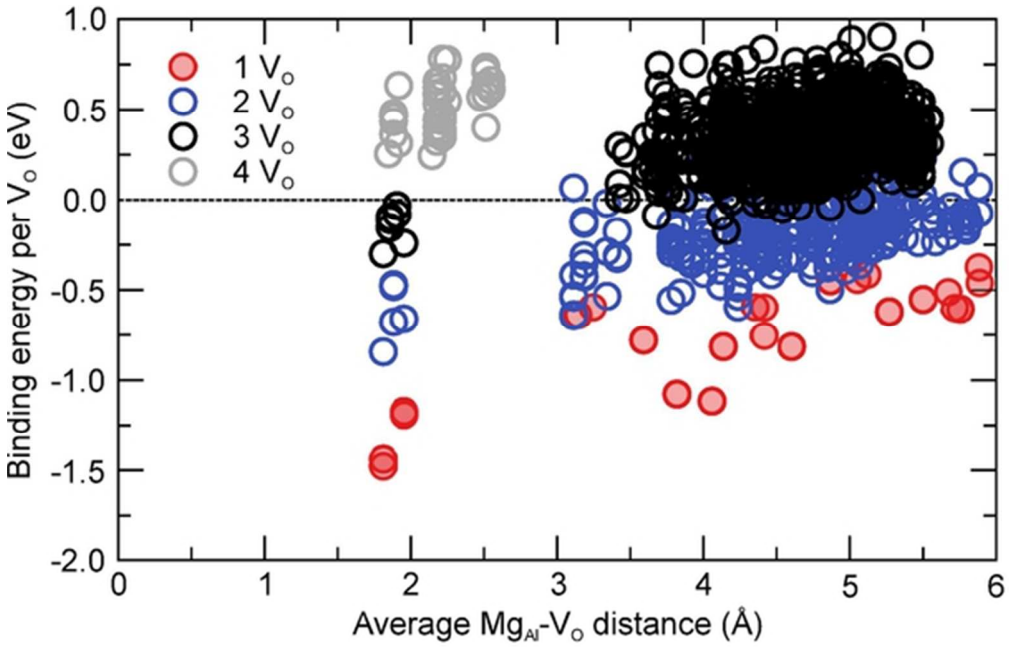

Figure 3. Binding energy per VO for defect clusters of one MgAl and one to four VO. Negative values indicate energetically favorable binding.
51x32mm (300 x 300 DPI)

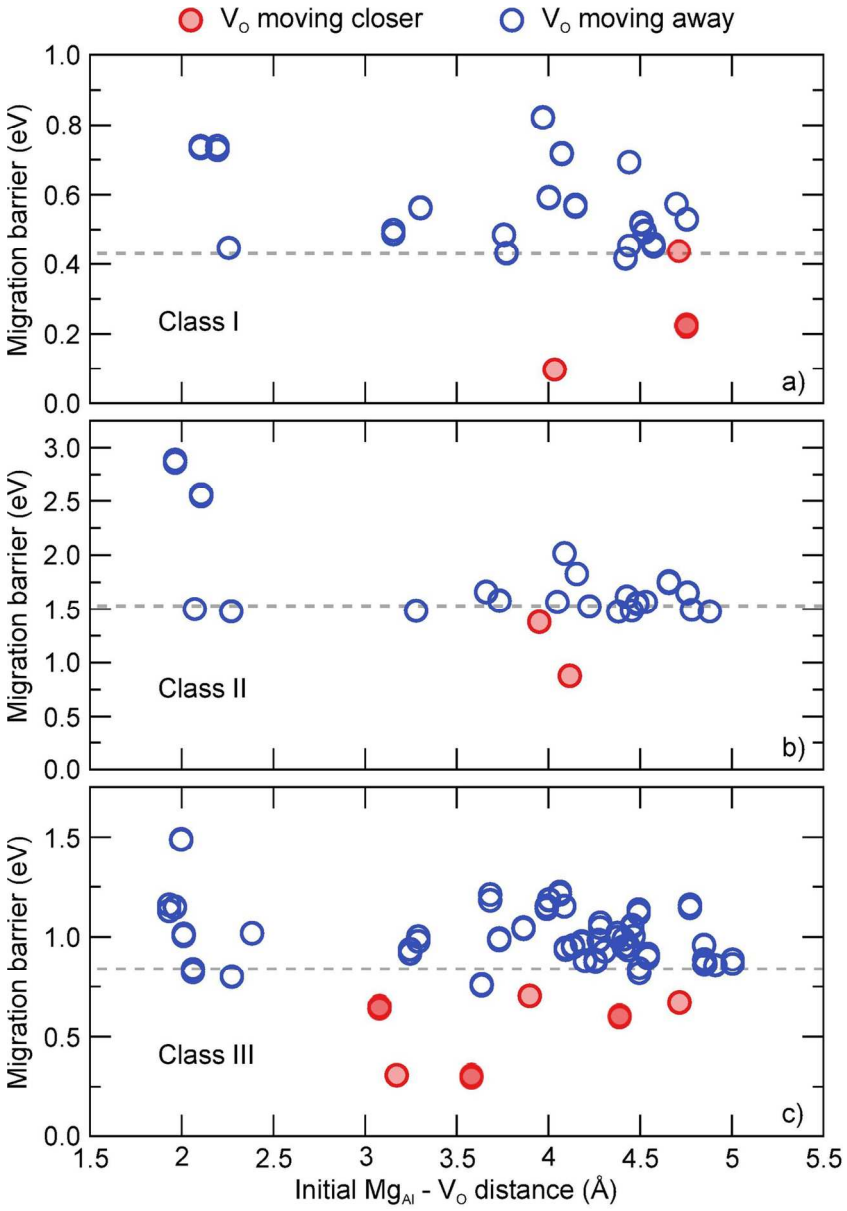

Figure 4. Migration barriers for the diffusive jumps of oxygen vacancies as a function of the initial distance of the oxygen vacancy from Mg for primary jumps of (a) class I (2.42 Å), (b) class II (2.54 Å) and (c) class III (2.65 Å). Dashed lines are the migration barriers in pure alumina for the respective class of jumps.
113x163mm (300 x 300 DPI)

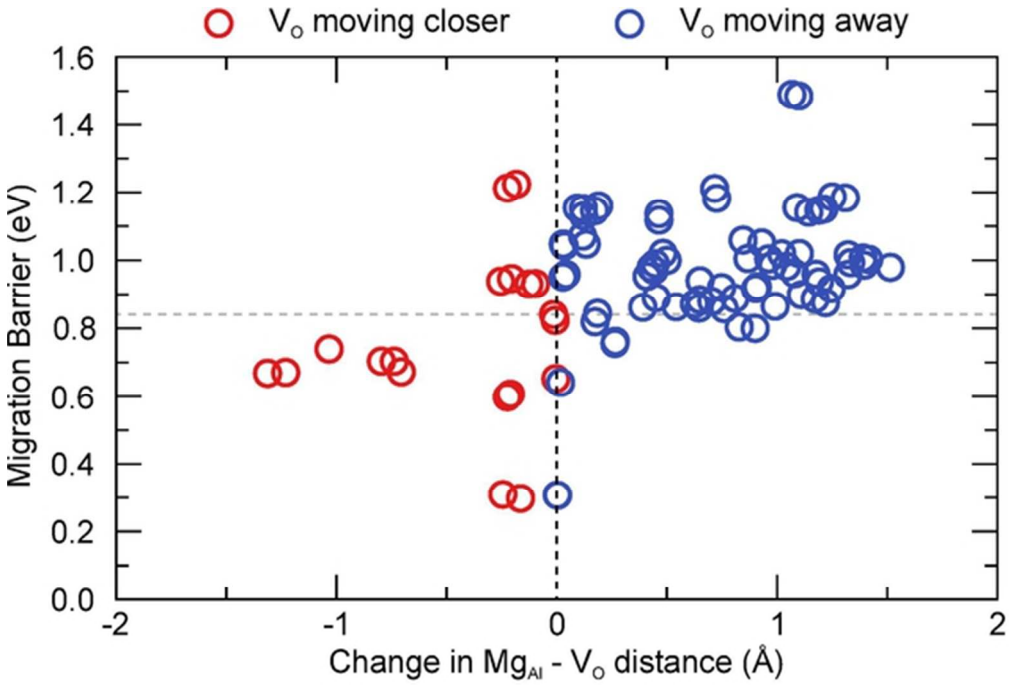

Figure 5. Migration barriers of class III diffusive jumps as a function of the difference in the initial and saddle point distance of the VO from MgAl. Negative values on the x-axis represent jumps where VO approaches MgAl. The dashed line is the migration barrier in pure alumina.
53x36mm (300 x 300 DPI)

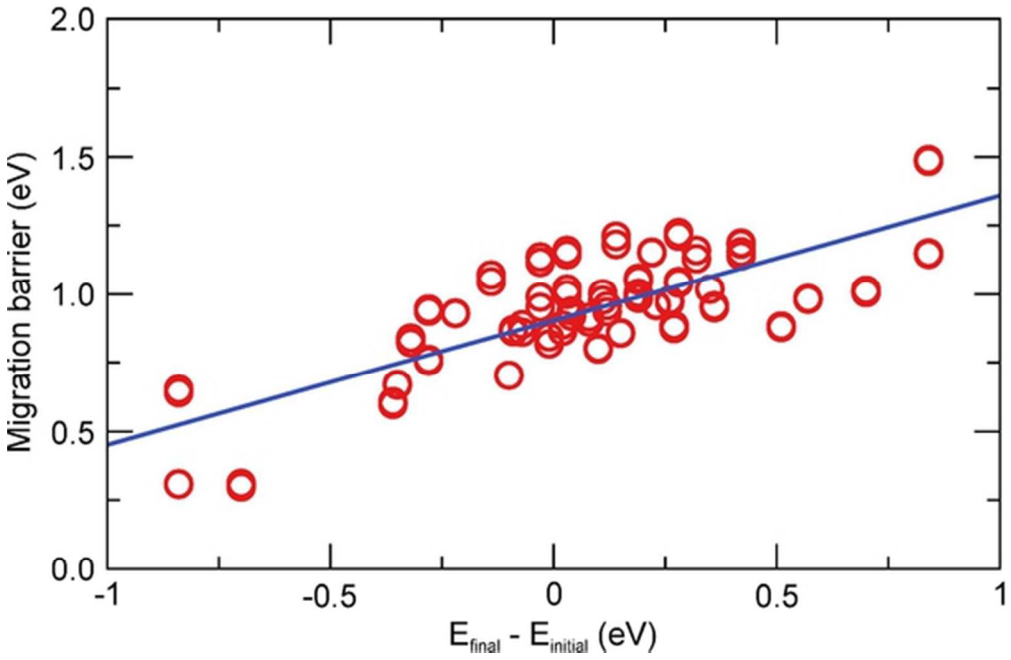

Figure 6. Brønsted-Evans-Polanyi plot. Migration barriers for the class III diffusive jumps plotted as a function of the energy difference between the initial and the final state of the vacancy. The straight line is a linear fit to the data points.
51x33mm (300 x 300 DPI)

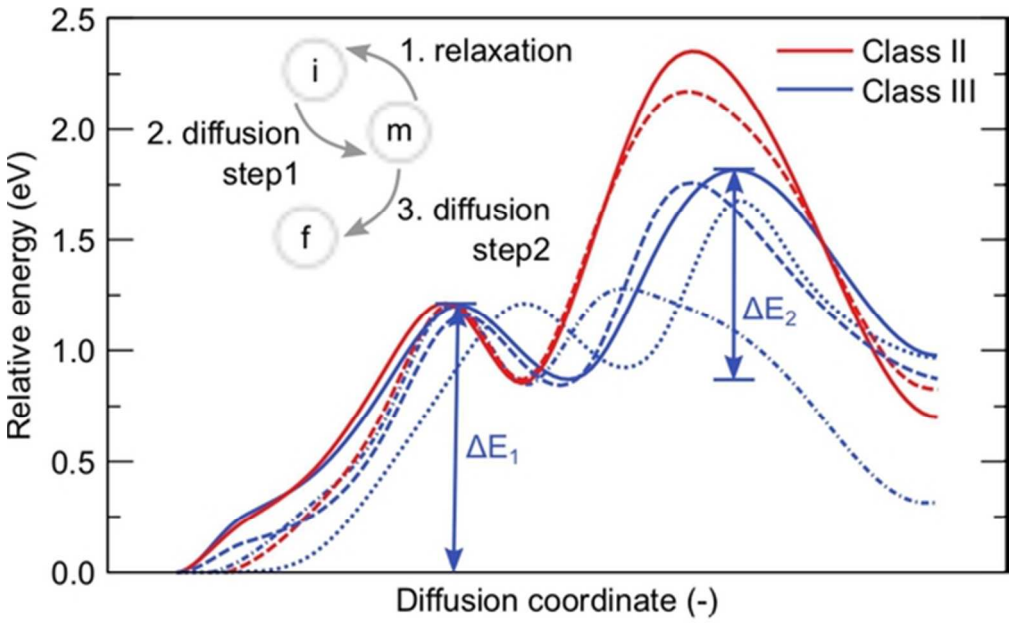

Figure 7. Minimum energy pathways for jumps starting from vacancy positions, which became unstable due to the presence of MgAl. The inset shows a schematic view of the relaxation process leading from the metastable (m) position to the new initial (i) position. Going from the new initial (i) position to the final (f) position now requires two diffusive jumps going via the intermediate metastable (m) state. This two-step nature is reflected by the two barriers observed in the minimum energy pathways (MEPs). The lines are cubic splines interpolated between NEB images. Red and blue solid curves are the MEPs of the highest barrier class II and class III jumps, respectively from this initial position. Red and blue dotted lines are the remaining class II and class III jumps respectively.
49x30mm (300 x 300 DPI)

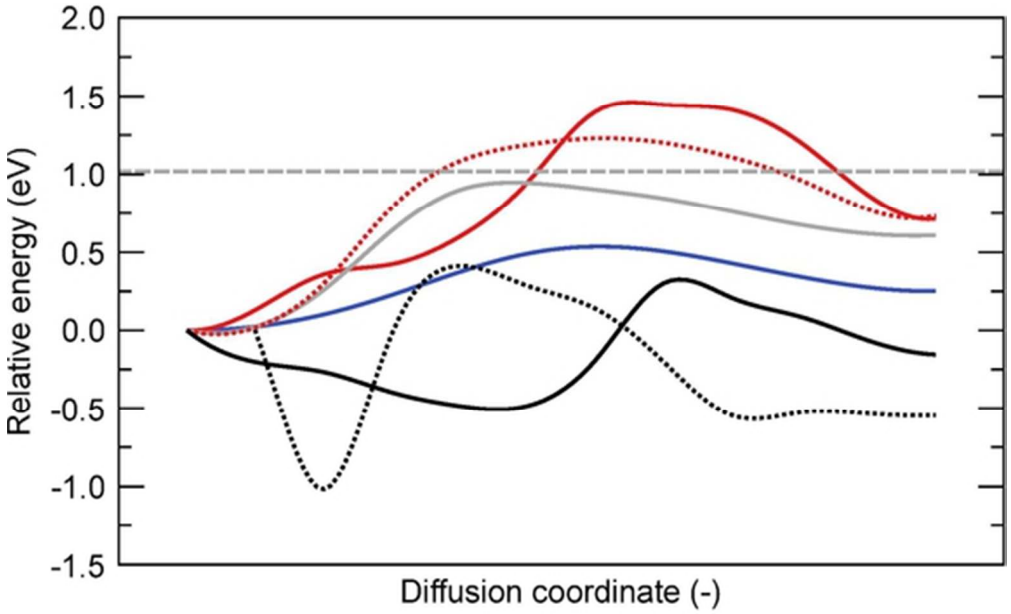

Figure 8. Minimum energy pathways showing the effect of VO-VO interaction by addition of a second VO at different nearest neighbor sites. The dashed horizontal line is the migration barrier of the jump without a second VO. Pathways with a destabilized initial position are shown in black, those with an increase in barrier in red, the one with an unaffected barrier in grey and the one with a lower barrier in blue. The lines are cubic splines interpolated between NEB images.
48x29mm (300 x 300 DPI)

Supplementary information for

Atomistic Modeling of Effect of Mg on Oxygen Vacancy Diffusion in α-Alumina

Abhishek Tewari[a,1], Ulrich Aschauer[b], Paul Bowen[a]

[a]Powder Technology Laboratory, Institute of Materials Science, EPFL, CH-1015 Lausanne, Switzerland

[b]Materials Theory, Department of Materials, ETH Zurich, CH-8093 Zürich, Switzerland

S1. Migration barrier variations

The potential model chosen in the present work[1] leads to an underestimation of the c lattice parameter (12.43 Å) compared to experiment (12.99 Å). In order to quantify the effect of this underestimation on the migration barriers, we have performed two additional sets of calculations: 1) using a potential set, which gives a c lattice parameter (12.72 Å) closer to experiment[2] and 2) using first-principles density functional theory (DFT) calculations, which are closest to the experimental lattice (12.93 Å). Calculations with the additional potential set were performed as described in the main text using the GULP[3] code with 10 intermediate images. DFT calculations were carried out using the Quantum ESPRESSO package[4] using ultra-soft pseudo-potentials[5] with Al 3s, 3p and O 2s, 2p as valence states. We employed the gradient corrected PBE[6] functional and expanded wave functions in plane-waves up to the kinetic energy of 25 Ry in conjunction with 200 Ry for the augmented density. Calculations were performed in a 2x2x1

[1] Corresponding author email: abhit1985@gmail.com

supercell (120 atoms) of the hexagonal unit-cell and reciprocal space was sampled using a 4x4x2 gamma centered mesh. For calculations with vacancies, a total charge of +2e was imposed via a uniform background charge. This corresponds to removing the two extra electrons together with the oxygen atom, which is the situation in the classical calculations. We want to note that calculations without this charge adjustment result in much larger migration energies of ~4.3 eV for class 3 jumps, which is in agreement with other DFT calculations performed using the unadjusted setup[7]. Due to the computational cost, only 5 intermediate images were used for DFT NEB calculations.

In Figure S1, we show the barriers for all three classes of jumps computed using the two additional methods and for reference we also repeat the Lewis potential[1] barriers already reported in the main text. We can see that the Lewis potential generally results in barriers, which are ~0.5 eV lower than the ones obtained using the Binks potential. It is however difficult to judge how much of this difference is caused by the expansion of the lattice and how much is caused by the different potential parameters. Additional calculations (not shown here) reveal that the class 1 and 2 jumps migration barriers are decreased, whereas for the class 3 jump it is increased, when the lattice parameter is expanded. This leads us to believe that the systematic increase observed for all the classes of jumps in Figure S1 is largely due to the different lattice parameters.

Looking at the DFT results in Figure S1 we can see that for jumps 1 and 3 an increase of the barrier by 0.25 and 0.5 eV respectively is predicted compared to the Binks potential. For class 2 the Binks potential barrier however almost coincides with the DFT results.

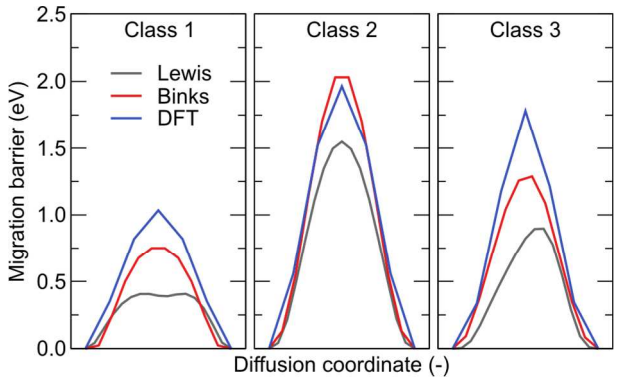

Figure S1: Migration barriers computed using the Lewis setup, which was used in the main text, compared to results obtained with the Binks potential and DFT calculations.

While we judge DFT calculations to be the most accurate for the determination of barriers, these results show that the computation of absolute values for barriers and hence a direct quantitative comparison with activation energies derived from experiment is affected by an uncertainty. This uncertainty stems from both changes in lattice geometry and changes in energetics from method to method. We thus conclude that absolute values should be taken with care. We will however establish in the following that relative changes are well described and that the effects of Mg on diffusion, as predicted in the main text, are valid.

S2. Relative changes

In order to assess how the uncertainty on lattice parameters and energetics affect the relative effect of a Mg impurity, we have computed the change in migration barriers when going from the pure alumina to the Mg doped system. These calculations were performed using both the Lewis[1] and the Binks[2] potential parameters at their respective lattice parameters. The results for the test set are shown in Figure S2. As we can see the change in the migration barrier is predicted to have very similar values for the two potential sets, the Binks potential generally predicting

slightly more marked changes. The largest deviations seem to occur for the cases where changes are largest.

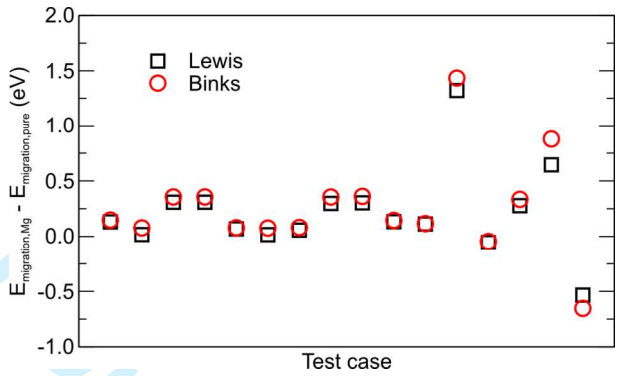

Figure S2: Change in migration barrier induced by the presence of Mg close to an oxygen vacancy. Results shown are for a small set of test cases.

The good agreement between the two potential sets at different lattice parameters gives us the confidence that although, as shown above, absolute values are affected by an uncertainty, relative changes are predicted consistently. A comparison with DFT calculations would be computationally very costly and therefore has not been done here.

S3. Effect of Mg-Vo-Mg cluster on migration barriers

Besides the V_O-Mg-V_O clusters treated in the main text, Mg-V_O-Mg clusters may also form. Formation of these clusters however requires the diffusion of Mg towards an existing Mg-V_O cluster. We have computed the migration barriers of Mg_{Al} in bulk alumina and found 1.13, 1.70 and 1.65 eV for the different nearest neighbor jumps. This is significantly higher than the migration barriers for V_O in alumina (0.84 eV, see main text) and the formation of Mg-V_O-Mg clusters should hence be kinetically less favorable than the formation of V_O-Mg-V_O clusters.

Few preliminary calculations were done in order to check the effect of Mg-Vo-Mg cluster formation on the migration barriers of the diffusive jumps. A set of oxygen vacancy diffusive jumps were carried out by substituting two Mg atoms at the nearest neighbor sites and the migration barriers were compared with the migration barriers of the jumps with only one substituted Mg atom present in the lattice. Although the migration barrier of a couple of jumps increased in presence of 2 Mg atoms in comparison to single Mg substitutional atom, the migration barriers of the other jumps were not affected much. These preliminary calculations point out that Mg-Vo-Mg may also affect the migration barriers of some diffusive jumps. However, the detailed study of the issue is out of the scope of the current work, but certainly requires more investigation in the future.

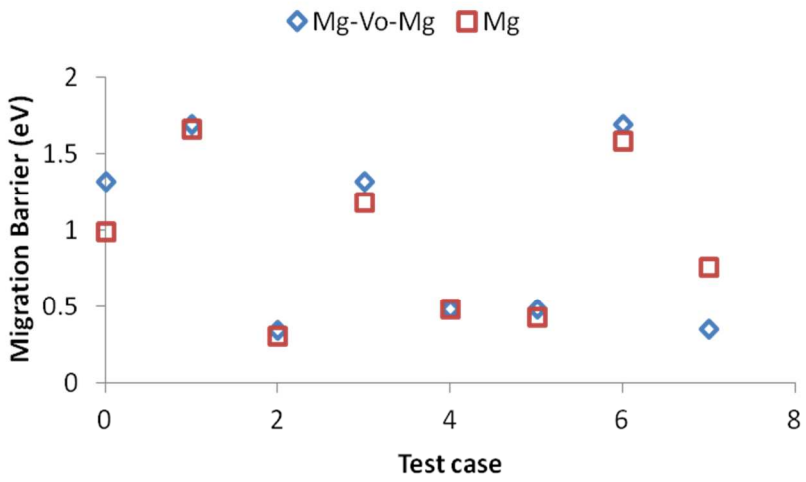

Figure S3: Change in migration barrier induced by the presence of 2 Mg atoms instead of only 1 Mg atom. Results shown are for a small set of test cases.

References

[1] G.V. Lewis and C.R.A. Catlow, "Potential models for ionic oxides," *J. Phys. C Solid State Phys.*, **18** [6] 1149–1161 (1985).

[2] D.J. Binks, "Computational Modelling of Zinc Oxide and Related Oxide Ceramics."; University of Surrey, Guildford, UK, 1994.

[3] J.D. Gale and A.L. Rohl, "The General Utility Lattice Program (GULP)," *Mol. Simul.*, **29** [5] 291–341 (2003).

[4] P. Giannozzi, S. Baroni, N. Bonini, M. Calandra, R. Car, C. Cavazzoni, D. Ceresoli, G.L. Chiarotti, *et al.*, "QUANTUM ESPRESSO: a modular and open-source software project for quantum simulations of materials," *J. Phys. Condens. Matter*, **21** [39] 395502 (2009).

[5] D. Vanderbilt, "Soft self-consistent pseudopotentials in a generalized eigenvalue formalism," *Phys. Rev. B*, **41** [11] 7892–7895 (1990).

[6] J.P. Perdew, K. Burke, and M. Ernzerhof, "Generalized Gradient Approximation Made Simple," *Phys. Rev. Lett.*, **77** [18] 3865–3868 (1996).

[7] Y. Lei, Y. Gong, Z. Duan, and G. Wang, "Density functional calculation of activation energies for lattice and grain boundary diffusion in alumina," *Phys. Rev. B*, **87** [21] 214105 (2013).

ELSEVIER LICENSE
TERMS AND CONDITIONS

Apr 07, 2014

This is a License Agreement between Abhishek Tewari ("You") and Elsevier ("Elsevier") provided by Copyright Clearance Center ("CCC"). The license consists of your order details, the terms and conditions provided by Elsevier, and the payment terms and conditions.

All payments must be made in full to CCC. For payment instructions, please see information listed at the bottom of this form.

Supplier	Elsevier Limited The Boulevard,Langford Lane Kidlington,Oxford,OX5 1GB,UK
Registered Company Number	1982084
Customer name	Abhishek Tewari
Customer address	EPFL-STI-IMX-LTP Lausanne, 1025
License number	3363770984378
License date	Apr 07, 2014
Licensed content publisher	Elsevier
Licensed content publication	Acta Materialia
Licensed content title	Oxygen vacancy diffusion in alumina: New atomistic simulation methods applied to an old problem
Licensed content author	U. Aschauer,P. Bowen,S.C. Parker
Licensed content date	September 2009
Licensed content volume number	57
Licensed content issue number	16
Number of pages	8

Start Page	4765
End Page	4772
Type of Use	reuse in a journal/magazine
Requestor type	author of new work
Intended publisher of new work	Wiley
Portion	figures/tables/illustrations
Number of figures/tables /illustrations	1
Format	both print and electronic
Are you the author of this Elsevier article?	Yes
Will you be translating?	No
Title of the article	Atomistic Modeling of Effect of Mg on Oxygen Vacancy Diffusion in α-Alumina
Publication new article is in	Journal of the American Ceramic Society
Publisher of the new article	Wiley
Author of new article	Abhishek Tewari, Ulrich Aschauer, Paul Bowen
Expected publication date	May 2014
Estimated size of new article (number of pages)	8
Elsevier VAT number	GB 494 6272 12
Permissions price	0.00 USD
VAT/Local Sales Tax	0.00 USD / 0.00 GBP
Total	0.00 USD
Terms and Conditions	

INTRODUCTION

1. The publisher for this copyrighted material is Elsevier. Byclicking "accept" in connection with completing this licensingtransaction, you agree that the following terms and conditions

apply to thistransaction (along with the Billing and Payment terms and conditionsestablished by Copyright Clearance Center, Inc. ("CCC"), at the timethat you opened your Rightslink account and that are available at any time at http://myaccount.copyright.com).

GENERAL TERMS

2. Elsevier hereby grants you permission to reproduce the aforementionedmaterial subject to the terms and conditions indicated.

3. Acknowledgement: If any part of the material to be used (for example,figures) has appeared in our publication with credit or acknowledgement toanother source, permission must also be sought from that source. If suchpermission is not obtained then that material may not be included in yourpublication/copies. Suitable acknowledgement to the source must be made, eitheras a footnote or in a reference list at the end of your publication, asfollows:

“Reprinted from Publication title, Vol /edition number, Author(s), Title ofarticle / title of chapter, Pages No., Copyright (Year), with permission fromElsevier [OR APPLICABLE SOCIETY COPYRIGHT OWNER].” Also Lancet special credit -“Reprinted from The Lancet, Vol. number, Author(s), Title of article, PagesNo., Copyright (Year), with permission from Elsevier.”

4. Reproduction of this material is confined to the purpose and/or media forwhich permission is hereby given.

5. Altering/Modifying Material: Not Permitted. However figures andillustrations may be altered/adapted minimally to serve your work. Any otherabbreviations, additions, deletions and/or any other alterations shall be madeonly with prior written authorization of Elsevier Ltd. (Please contact Elsevierat permissions@elsevier.com)

6. If the permission fee for the requested use of our material is waived inthis instance, please be advised that your future requests for Elseviermaterials may attract a fee.

7. Reservation of Rights: Publisher reserves all rights not specificallygranted in the combination of (i) the license details provided by you andaccepted in the course of this licensing transaction, (ii) these terms andconditions and (iii) CCC's Billing and Payment

terms and conditions.

8. License Contingent Upon Payment: While you may exercise the rightslicensed immediately upon issuance of the license at the end of the licensingprocess for the transaction, provided that you have disclosed complete andaccurate details of your proposed use, no license is finally effective unlessand until full payment is received from you (either by publisher or by CCC) asprovided in CCC's Billing and Payment terms and conditions. If fullpayment is not received on a timely basis, then any license preliminarilygranted shall be deemed automatically revoked and shall be void as if nevergranted. Further, in the event that you breach any of these terms andconditions or any of CCC's Billing and Payment terms and conditions, thelicense is automatically revoked and shall be void as if never granted. Use of materials as described in a revoked license, as well as any use of thematerials beyond the scope of an unrevoked license, may constitute copyrightinfringement and publisher reserves the right to take any and all action toprotect its copyright in the materials.

9. Warranties: Publisher makes no representations or warranties with respectto the licensed material.

10. Indemnity: You hereby indemnify and agree to hold harmless publisher andCCC, and their respective officers, directors, employees and agents, from andagainst any and all claims arising out of your use of the licensed materialother than as specifically authorized pursuant to this license.

11. No Transfer of License: This license is personal to you and may not besublicensed, assigned, or transferred by you to any other person withoutpublisher's written permission.

12. No Amendment Except in Writing: This license may not be amended exceptin a writing signed by both parties (or, in the case of publisher, by CCC onpublisher's behalf).

13. Objection to Contrary Terms: Publisher hereby objects to any termscontained in any purchase order, acknowledgment, check endorsement or otherwriting prepared by you, which terms are inconsistent with these terms andconditions or CCC's Billing and Payment terms and conditions. These termsand conditions, together with CCC's Billing and Payment terms and conditions(which are incorporated herein), comprise the entire agreement between you andpublisher (and CCC) concerning this licensing transaction. In the eventof any

conflict between your obligations established by these terms andconditions and those established by CCC's Billing and Payment terms andconditions, these terms and conditions shall control.

14. Revocation: Elsevier or Copyright Clearance Center may deny thepermissions described in this License at their sole discretion, for any reasonor no reason, with a full refund payable to you. Notice of such denialwill be made using the contact information provided by you. Failure toreceive such notice will not alter or invalidate the denial. In no eventwill Elsevier or Copyright Clearance Center be responsible or liable for anycosts, expenses or damage incurred by you as a result of a denial of yourpermission request, other than a refund of the amount(s) paid by you toElsevier and/or Copyright Clearance Center for denied permissions.

LIMITED LICENSE

The following terms and conditions apply only to specific license types:

15. **Translation**: This permission is granted fornon-exclusive world **English** rights only unless yourlicense was granted for translation rights. If you licensed translation rightsyou may only translate this content into the languages you requested. Aprofessional translator must perform all translations and reproduce the contentword for word preserving the integrity of the article. If this license is tore-use 1 or 2 figures then permission is granted for non-exclusive world rightsin all languages.

16. **Posting licensed content on any Website**: The followingterms and conditions apply as follows: Licensing material from an Elsevierjournal: All content posted to the web site must maintain the copyright informationline on the bottom of each image; A hyper-text must be included to the Homepageof the journal from which you are licensing at http://www.sciencedirect.com/science/journal/xxxxx orthe Elsevier homepage for books at http://www.elsevier.com; CentralStorage: This license does not include permission for a scanned version of thematerial to be stored in a central repository such as that provided byHeron/XanEdu.

Licensing material from an Elsevier book: A hyper-text link must be includedto the Elsevier homepage at http://www.elsevier.com . Allcontent posted to the web site must maintain the copyright information line onthe bottom of each image.

Posting licensed content on Electronic reserve: In addition to the above the following clausesare applicable: The web site must be password-protected and made available onlyto bona fide students registered on a relevant course. This permission isgranted for 1 year only. You may obtain a new license for future websiteposting.

For journal authors: the following clauses are applicable inaddition to the above: Permission granted is limited to the author acceptedmanuscript version* of your paper.

***Accepted Author Manuscript (AAM) Definition:** An accepted authormanuscript (AAM) is the author's version of the manuscript of an article thathas been accepted for publication and which may include any author-incorporatedchanges suggested through the processes of submission processing, peer review,and editor-author communications. AAMs do not include other publishervalue-added contributions such as copy-editing, formatting, technicalenhancements and (if relevant) pagination.

You are not allowed to download and post the published journal article (whetherPDF or HTML, proof or final version), nor may you scan the printed edition tocreate an electronic version. A hyper-text must be included to the Homepage ofthe journal from which you are licensing at http://www.sciencedirect.com/science/journal/xxxxx. As part of our normal production process, you will receive an e-mail noticewhen your article appears on Elsevier's online service ScienceDirect(www.sciencedirect.com). That e-mail will include the article's Digital ObjectIdentifier (DOI). This number provides the electronic link to the publishedarticle and should be included in the posting of your personal version. We askthat you wait until you receive this e-mail and have the DOI to do any posting.

Posting to a repository: Authorsmay post their AAM immediately to their employer's institutional repository forinternal use only and may make their manuscript publically available after thejournal-specific embargo period has ended.

Please also refer to Elsevier'sArticle Posting Policy for further information.

18. **For book authors** the following clauses are applicable in addition tothe above: Authors are permitted to place a briefsummary of their work online only.. You are notallowed to download and post the published electronic version of your chapter,nor may you scan the printed edition to create an electronic version. Posting to a repository: Authors arepermitted

to post a summary of their chapter only in their institution'srepository.

20. **Thesis/Dissertation**: If your license is for use in athesis/dissertation your thesis may be submitted to your institution in eitherprint or electronic form. Should your thesis be published commercially, pleasereapply for permission. These requirements include permission for the Libraryand Archives of Canada to supply single copies, on demand, of the completethesis and include permission for UMI to supply single copies, on demand, ofthe complete thesis. Should your thesis be published commercially, pleasereapply for permission.

Elsevier Open Access Terms andConditions

Elsevier publishes Open Access articles in both its Open Access journals andvia its Open Access articles option in subscription journals.

Authors publishing in an Open Access journal or who choose to make theirarticle Open Access in an Elsevier subscription journal select one of thefollowing Creative Commons user licenses, which define how a reader may reusetheir work: Creative Commons Attribution License (CC BY), Creative CommonsAttribution – Non Commercial - ShareAlike (CC BY NCSA) and Creative Commons Attribution – Non Commercial – No Derivatives (CC BYNC ND)

Terms & Conditions applicable toall Elsevier Open Access articles:

Any reuse of the article must not represent the author as endorsing theadaptation of the article nor should the article be modified in such a way asto damage the author's honour or reputation.

The author(s) must be appropriately credited.

If any part of the material to be used (for example, figures) has appearedin our publication with credit or acknowledgement to another source it is theresponsibility of the user to ensure their reuse complies with the terms andconditions determined by the rights holder.

Additional Terms & Conditionsapplicable to each Creative Commons user license:

CC BY: You may distribute andcopy the article, create extracts, abstracts, and other revised versions,adaptations or derivative works of or from an article (such as a translation),to include in a collective work (such as an anthology), to text or data minethe article, including for commercial purposes without permission from Elsevier

CC BY NC SA: For non-commercialpurposes you may distribute and copy the article, create extracts, abstractsand other revised versions, adaptations or derivative works of or from anarticle (such as a translation), to include in a collective work (such as ananthology), to text and data mine the article and license new adaptations or creationsunder identical terms without permission from Elsevier

CC BY NC ND: For non-commercialpurposes you may distribute and copy the article and include it in a collectivework (such as an anthology), provided you do not alter or modify the article,without permission from Elsevier

Any commercial reuse of Open Access articles published with a CC BY NC SA or CC BY NC NDlicense requires permission from Elsevier and will be subject to a fee.

Commercial reuse includes:

- Promotional purposes (advertising or marketing)
- Commercial exploitation (e.g. a product forsale or loan)
- Systematic distribution (for a fee or free ofcharge)

Please refer to Elsevier'sOpen Access Policy for further information.

21. **Other Conditions**:

v1.7

If you would like to pay for this license now, please remit this license along with your payment made payable to "COPYRIGHT CLEARANCE CENTER" otherwise you will be invoiced within 48 hours of the license date. Payment should be in the form of a check or money order referencing your account number and this invoice number RLNK501271795.
Once you receive your invoice for this order, you may pay your invoice by credit card. Please follow instructions provided at that time.

Make Payment To:
Copyright Clearance Center
Dept 001
P.O. Box 843006
Boston, MA 02284-3006

For suggestions or comments regarding this order, contact RightsLink Customer Support: customercare@copyright.com or +1-877-622-5543 (toll free in the US) or +1-978-646-2777.

Gratis licenses (referencing $0 in the Total field) are free. Please retain this printable license for your reference. No payment is required.